Nanoscale

Accepted Manuscript

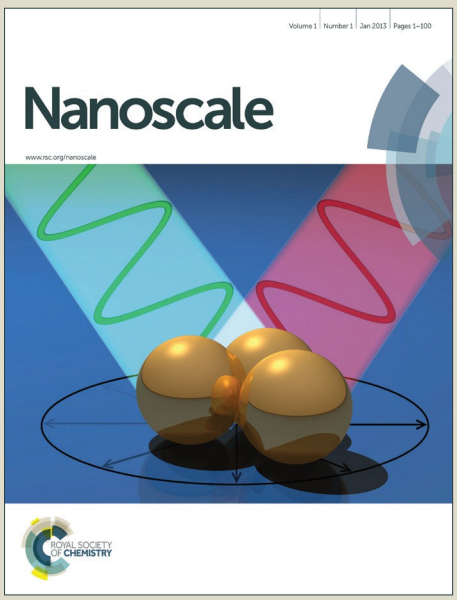

ROYAL SOCIETY OF CHEMISTRY

www.rsc.org/nanoscale

Journal Name

ARTICLE TYPE

Cite this: DOI: 10.1039/xxxxxxxxxx

Field-directed assembly of nanowires: identifying directors, disruptors and indices to maximize device yield

Mahshid Sam,[a] Nima Moghimian,[a] and Rustom B. Bhiladvala *[a]

Received Date
Accepted Date

DOI: 10.1039/xxxxxxxxxx

www.rsc.org/journalname

Individually-addressable nanomechanical (NEMS) devices have been used to demonstrate sensitive mass detection to single-proton level, as well as neutral-particle mass spectrometry. The cost of individually securing or patterning such devices is proportional to their number or the chip area covered. This limits statistical support for research results, as well as paths to the commercial availability of extraordinarily sensitive instruments. Field-directed assembly of synthesized nanowires addresses this problem and shows potential for low-cost, large-area coverage with NEMS devices. For positive dielectrophoresis (pDEP) as the main assembly director, the space of field, geometric and material parameters is large, with combinations that can serve either as directors or disruptors for directed assembly. We seek parameter values to obtain the best yield, by introducing a rational framework to reduce trial-and-error. We show that sorting the disruptors by severity and eliminating those weakly coupled to the director, allows a reduction of parameter space. The remaining disruptors are then represented compactly by dimensionless parameters. In the example protocol chosen, a single dimensionless parameter, the yield index, allows minimization of disruptors by the choice of frequency. Following this, the voltage may be selected to maximize yield. Using this framework, we obtained 94% pre-clamped and 88% post-clamped yield at 57000 nanowire sites. Organizing the parameter space using a director-disruptor framework, with economy introduced by non-dimensional parameters, provides a path to controllably decrease the effort and cost of manufacturing nanoscale devices. This should help in the commercialization of individually addressable nanodevices.

1 Introduction

Remarkable capabilities of single-proton mass detection [1], neutral particle mass spectrometry [2] and earlier, the detection of nucleic acid sequences [3] have been demonstrated using individually addressable nanomechanical (NEMS) devices, but only for a small number of clamped nanowires (NWs) or nanobeams. Large-area coverage with individually-addressable NW devices will significantly reduce experimental research time for future landmark demonstrations. If done at low cost, it will also enable stronger statistical support for measurements needed to understand mechanical [4–7] and electrical [4,8,9] behavior of NWs, and most significantly, ease the development of instruments for commercial applications, such as screening for early detection of disease through molecular diagnosis [10]. A recent review [11] provides several examples of promising NW device applications.

Directed assembly provides a path towards nanomanufacturing systems to achieve large-area coverage at low-cost. For nanofabrication, the term directed assembly describes a family of methods [12–16] which use micro-patterned structures for spatial and temporal control of fields, to direct synthesized nanoscale elements to predetermined locations. The patterned structures enable NW position control and could involve one of several *fields* -such as hydrodynamic, electric, magnetic, temperature -or their combinations. Such field-directed assembly combines elements of top-down microfabrication and bottom-up nanostructure synthesis, enabling fabrication of nanoscale devices in large arrays. It retains the advantages of using low-cost nanostructure assembly (compared to electron-beam lithographic patterning) offered by self-assembly [16,17], but also provides greatly improved position control, and a route to individual device addressability.

In contrast with established macroscale manufacturing processes, research laboratory nanofabrication protocols, including field-directed assembly, often require some small modifications to

[a] *Department of Mechanical Engineering, Center for Advanced Materials and Related Technologies (CAMTEC) and Integrated Energy Systems at the University of Victoria (IESVic), University of Victoria, Victoria, BC, Canada. E-mail: rustomb@uvic.ca*

† Electronic Supplementary Information (ESI) available: [This section includes micrographs of high yield pre- and post- clamped nanowires]. See DOI: 10.1039/b000000x/

be reproducible by a new user or in a new facility. These changes are a consequence of unknown methods or prohibitive cost of adequate metrology at and below device scales, during each fabrication step. In addition, there is an imperfect understanding of possible coupling between several physical effects, as discussed in the example protocol chosen for this paper. As a result, a user who decides to change a single step, material or experimental parameter value within a protocol may often have to change several others. In the absence of a framework to guide the choice of experimental parameter values, considerable effort is spent in a trial-and-error approach to obtain best yield from NW assembly. To strongly reduce such effort, we propose a framework, based on identifying forces, which serve either as *directors* or *disruptors*, with competing effects on yield in directed assembly. The framework provides a rational guide to parameter value selection.

Dielectrophoresis (DEP) force has been reported by a few research laboratories[9,12–15,18–21] worldwide, as a director in field-directed NW assembly. Examples of directors and disruptors are forces that arise from negative or positive DEP[21], Brownian motion[22,23], electroosmotic forces[14,20] or electrode polarization effects[14,18]. Here we use a sequence of basic steps from a known DEP protocol, reported in the work of Li *et al.*[15], to help illustrate the utility of the framework. Starting with an established basis is also necessary to examine whether any improvements in yield accrue from use of the framework.

While parameter values are chosen using the framework developed later in this paper, here we briefly outline the basic steps utilized, as shown in Fig. 1(a) to (d). We used rhodium (Rh) NWs that have desirable mechanical properties for resonant mass sensing as they retain high quality factor (Q-factor) from high vacuum to near atmospheric pressure[15]. Photolithography was first used to create electrically conductive pad pairs with different gap widths of 6, 8 and 10 μm, which define the locations to which NWs will be directed. A photoresist layer was spun to cover the electrodes and prevent an electrical short circuit that would result from NWs bridging electrode pads. Wells (shown in Fig. 1(a)) were then patterned in photoresist between each electrode pair, followed by application of the electric field to direct NWs into wells (Fig. 1(b)). Photoresist was removed from one of the electrode pairs and clamp material was electrodeposited to fix one end of the NWs (Fig. 1(c)). Finally, NWs were suspended by removing the remaining photoresist from the substrate and using critical point drying. Experimental details may be found in Section 4 at the end of this paper.

The word "yield" in the literature on directed assembly has been used to refer to different things. Most devices made from suspended NWs need one or both ends to be clamped after the directed assembly process is complete. Though clamping processes typically do reduce the yield, the word "yield" has been used to report the yield from assembly alone[12,19], while other reports[15] use the word to mean yield of functional devices after both assembly and clamping. It is misleading to compare numbers for the yield between these two groups of references. To avoid confusion, we suggest the use of two categories of NW yield: pre-clamped yield, which is the percent of available sites with correctly positioned single NWs; and post-clamped yield, referring to the percent of sites with functional, clamped NWs.

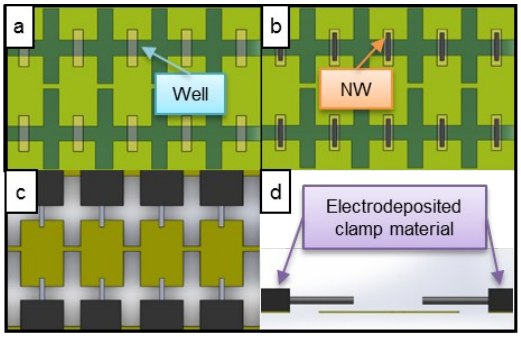

Fig. 1 Schematics of positioning and clamping of single NWs on gold electrodes: (a) patterning electrode pairs with wells in between, to locate and trap NWs (b) positioning single NWs inside wells using DEP (c) electrodeposition of clamp material after photoresist removal from electrode surface (d) side view of clamped NWs after removing the remaining photoresist.

2 Framework development

This study is focused on developing a framework for field-directed assembly of NWs. A DEP protocol with positive dielectrophoresis (pDEP) as the main director is used here to show the framework methodology in classifying and evaluating the director and disruptors. We separate disruptors into two groups: {1} disruptors weakly coupled to the main director, pDEP, that either depend on electrode design or need less quantification to be eliminated and {2} disruptors that are strongly coupled through parameter choice to the main director. In this section, we first evaluate weakly-coupled disruptors (disruptive torque, capillary force from the drying front, improper NW concentration, Brownian motion and electrothermal force) followed by strongly-coupled ones (negative DEP (nDEP), electroosmotic force and electrode polarization). In this evaluation, the results of analysis and computation can provide useful guidance, even if somewhat rough. This step is followed by the definition of a dimensionless parameter, which compactly represents the competition between the director and the remaining disruptors. This helps to guide parameter value selection for best device yield, with reduced trial-and-error. In the example chosen in this study, the final control of device yield was realized only by tuning the director, with negligible hindrance from disruptors.

2.1 Weakly-coupled disruptors

2.1.1 Disruptive torque

DEP torque, a primary need for NW alignment, can become a disruptor when NWs are much longer than the width of the gap between electrodes, in each electrode pair. For low values of the ratio (λ) of electrode gap width to NW length, the induced dipoles can lie beyond the two electrode edges, rather than in between them, with a torque that rotates NWs in an opposite sense to that required for alignment (disruptive or "negative" torque). Some guidance is provided by the computational results of Liu *et al.*[22], which show that it is possible to avoid disruptive torque if $\lambda > 0.4$, that is, when NW length is smaller than 2.5 times the gap width.

NWs of length smaller than the gap width ($\lambda > 1$) clearly cannot have both ends clamped, and may produce one-end clamped devices which are outside of the intended functional range, even if they are properly aligned. To avoid this, we restrict our choices to the range ($0.4 < \lambda < 1$).

2.1.2 Capillary force

The spreading of a drop of NW suspension during assembly carries NWs beyond the target assembly region and often leads to undesirable spillover on adjacent dies. Vigorous NW motion was observed during such drop spreading, acting as a disruptor. A further disruptive role of capillary force was seen at drying fronts, that pull away NWs which are partially protruding from wells.

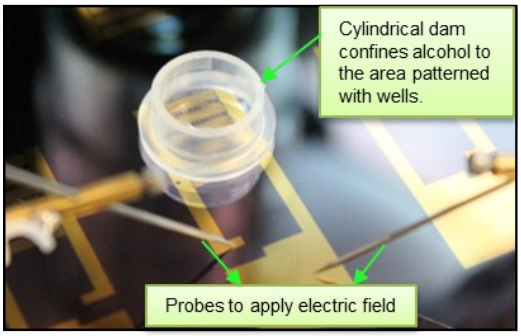

Fig. 2 A cylindrical dam reduces the effects of drying-front capillary force as a disruptor and prevents NW spillover to adjacent dies.

To reduce these disruptive effects, we introduced a cylindrical dam (Fig. 2) with 1 cm diameter and 0.5 cm height, which confined NW suspension to the area of one die with 9500 wells. This eliminates the spreading and flow disruption and leaves a sufficient excess time for DEP to secure both NW ends within wells.

2.1.3 Inappropriate nanowire concentration

Having too low a concentration will lead to unfilled sites. For any selected suspension volume, a concentration allowing at least one NW for each well (equivalent to 9.5×10^5 NW/mL) is clearly needed to avoid empty sites. However, too high a NW concentration can lead to the formation of chains, bundles, or multiple NWs assembled between electrode pairs, disrupting single-NW assembly and reducing yield. Using the procedure in Methods Section 4, we determined by experiment that a concentration of 19×10^5 NW/mL (2 NWs for each well) was suitable, and repeatedly allowed us to avoid problems associated with too high a concentration of NWs. Images of NW assembly with different NW concentration are provided in Fig S1†.

2.1.4 Brownian motion

In our experiments, random displacement of NWs due to Brownian motion was observed when no electric field was applied. However, when the electric field was applied, we observed NW trapping within wells begin in about a second after the NW suspension was introduced.

Inspite of our observation for this assembly process, we ask how significant a disruptor Brownian motion could be, and in what circumstances. Cumulative Brownian displacement could be disruptive if it is comparable to, or greater than the displacement due to the DEP force. It is less likely to be disruptive very close to the electrode edges, where the field gradient and DEP force are strongest, but has scope to disrupt motion along the capture path at large distances from the electrode. The ratio of the root-mean-squared (rms) NW displacement induced by Brownian motion to DEP displacement has been estimated earlier[22,23] for spherical particles. We obtain results for cylindrical NWs, moving perpendicular to the NW axis, in low Reynolds number flow. For this case, the drag coefficient is given by[24]

$$\gamma = F_d/u = 4\pi\eta L/[ln(2L/d) + 0.5] \quad (1)$$

Here L, d are the NW length and diameter respectively, the drag force is F_d, u is the velocity of the NW relative to the fluid and η is the dynamic viscosity of the fluid. With L=10μm, d=0.25μm and $\eta = 1.2\times10^{-3}$ Pa.s for ethanol, the drag coefficent value is 3.09×10^{-8} kg/s. The reader is referred to the steps in the Appendix of this manuscript, for derivation of the ratio of Brownian to DEP displacement, in elapsed time t, which yields,

$$\Delta X_{Br}/\Delta X_{DEP} = \sqrt{(2k_BT)/(u^2\gamma t)} = \sqrt{(2K_BT\gamma)/(F^2 t)} \quad (2)$$

Here F is the DEP force, k_B is Boltzmann's constant and absolute temperature T=293K. The ratio is inversely proportional to NW velocity, and decreases with elapsed time as $t^{-1/2}$. There is no known way of measuring forces, or velocities normal to the observation plane, for individual NWs during this assembly process, and we expect both will depend on NW height above electrodes. However, we may use Eq. (2) to examine the role of Brownian motion from an order of magnitude estimate. Fluid depth in the dam is $\sim$100 μm. An assembly time $\sim$1 s, for a distant NW in the vicinity of the fluid-air interface, yields an estimate for maximum NW velocity of $\sim$100 μm/s, for which the value of $\Delta X_{Br}/\Delta X_{DEP}$ is calculated to be 0.005. For a more reasonable starting NW distance of $\sim$10 μm, the velocity would be $\sim$10 μm/s, and this ratio would be 0.05. NWs at starting distances $\sim$1 μm or lower would be in the highest field gradient region and close to capture within the wells. In accord with our experimental observations, this rough estimation process confirms that Brownian motion is not a significant disruptor.

However, the value of this rough scaling analysis is that it shows Brownian motion could be a significant disruptor for slow-moving NWs, low DEP force and for liquids at low temperatures or with high viscosity.

2.1.5 Electrothermal force

Electrothermal force is another disruptor for DEP-assisted positioning of NWs. The current due to applied electric field causes local heat generation in the solution. The resulting temperature variation, if significant, would lead to conductivity and permittivity gradients in the fluid. Therefore, the force imposed on the medium by electric field can vary in different parts of the fluid and induce fluid flow, named electrothermal flow, which interacts with NW positioning. The fluid temperature change is given by[22,23]:

$$\Delta T \approx \frac{\sigma_m V_{rms}^2}{2K} \quad (3)$$

where K and σ_m are thermal and electrical conductivity of the fluid medium respectively (K =0.171 W.m^{-1}.K^{-1}and σ_m is 2.19×10^{-5} Sm^{-1} for ethanol[25]). The maximum applied voltage in this work, V_{rms} =7 V yields a temperature rise of about 10^{-3} °C. For this small temperature change, the effect on permittivity and conductivity is negligible and electrothermal fluid flow is not considered as a disruptor in this work.

In this section, we have used results of analysis and computation as a rough guide to (a) find which potential disruptors are negligible (here, Brownian motion and electrothermal force) and (b) impose constraints on physical parameters (such as ratio of electrode gap width to NW length) to make disruptors negligible. We also used experiments to eliminate some potential disruptors (capillary force and inappropriate NW concentration). Enforcing these constraints reduces the dimension of parameter space. If there is a resurgence of disruptors when modifications are made to established parameter values for a given protocol, these constraints provide a path for correction. This greatly reduces time spent compared to a trial-and-error approach with little intuition.

2.2 Strongly-coupled disruptors

2.2.1 Negative DEP

The time averaged DEP force is given by[21,26]:

$$F_{DEP} = \frac{\pi r^2 l}{6} \varepsilon_m Re[F_{CM}] . \bigtriangledown (E_l^2) \quad (4)$$

with

$$F_{CM} = \frac{\varepsilon_p^* - \varepsilon_m^*}{\varepsilon_m^*} \quad (5)$$

where l and r are the length and radius of a NW, ε_m is permittivity of the medium and E_l is the electric field. Re[F_{CM}], the real part of the Clausius-Mossotti factor, is positive over a range of frequencies for conductive NWs suspended in alcohol and becomes negative at sufficiently high frequencies[20,26].

ε_p^* and ε_m^* are the complex permittivity of NWs and medium respectively, defined as $\varepsilon^* = \varepsilon - j(\frac{\sigma}{\omega})$ where ω is the angular frequency of the applied electric field. The sign of Re[F_{CM}] dictates the sign of F_{DEP}. NWs can be attracted to or repelled from the wells when F_{DEP} is positive or negative, respectively. Here, we eliminate nDEP simply by choosing frequencies below 10^{10} Hz (Fig.3(b)), ensuring DEP remains solely a director. Later in this paper, we will see that other constraints on frequency compel us to use frequencies well below 10^{10} Hz.

2.2.2 Electroosmotic velocity

Among electrohydrodynamic (EHD) effects, a strong potential disruptor in this work is electroosmotic flow, which can interfere with NW positioning by creating a vortical flow, as shown in Fig. 3(a). This flow is driven by the electroosmotic force $F = qE_t$, where E_t is the tangential component of the electric field and q is the surface charge density of the electrical double layer. Green *et al.*[27] and Castellanos *et al.*[23] showed that electroosmotic fluid velocity strongly depends on the applied frequency. In addition, Eq. (5), plotted in Fig. 3(b), shows that Re[F_{CM}] and as a result F_{DEP}, also depend on frequency. We show below, that a careful choice of frequency can be used to overcome the disruptive effect of electroosmotic flow.

The electroosmotic velocity, v, can be calculated using[27]

$$v = \frac{\varepsilon_m V_{rms}^2}{4x\eta} \times \frac{\Omega^2}{(1+\Omega^2)^2} = \frac{\varepsilon_m V_{rms}^2}{4x\eta} f(\Omega) \quad (6)$$

knowing the rms-value of applied voltage (V_{rms}), dynamic viscosity of the electrolyte (η) and characteristic length x (half the gap width between electrodes), and with Ω, the dimensionless frequency, defined as:

$$\Omega = \frac{\pi}{2} x\kappa\omega(\frac{\varepsilon_m}{\sigma_m}) \quad (7)$$

where κ is the reciprocal Debye length of the double layer. For liquids with a low dielectric constant, such as ethanol, κ^{-1} is ∼0.5 μm[28]. Electroosmotic velocity is plotted in Fig. 3(c) for ethanol with ε_m=2.3 × 10^{-10} F.m^{-1} and σ_m = 2.19×10^{-5} Sm^{-1}, at V_{rms}=7 V and characteristic length of x =5 μm. It shows a frequency peak at ∼10^3 Hz, which is termed the EO-characteristic frequency. At low frequencies, here below ∼10^2 Hz, the voltage drop across the double layer is high, making E_t small, with the resulting electroosmotic force $F = qE_t$ being too small to create electroosmotic flow. At high frequencies, here above ∼4×10^4 Hz, we do not see electroosmotic flow, but for a different reason. At this high frequency the double layer does not have sufficient time to form[23,27], and the electroosmotic force is small because q is small. The calculation above provides guidance for selecting frequency to minimize electroosmotic flow. In addition, to enable use of a normalized electrosomotic velocity, (v/v_{max}), as a dimensionless measure of the strength of this disruptor, Eq. (7) shows that the maximum value of $f(\Omega)$ occurs at Ω=1, yielding v_{max} = $(\varepsilon_m V_{rms}^2)/(16x\eta)$. This parameter, v_{max}, will be used in Sec 2.4.

2.2.3 Electrode polarization

The presence of an electrical double layer gives rise to another disruptor, electrode polarization. Electrode polarization causes a voltage drop adjacent to the electrode, and as a result, the effective voltage (V_{eff}) that provides the field strength for NW positioning, becomes less than the applied voltage (V_{rms}). The electrical conduction path, shown in Fig. 3(d) (inset) consists of electrolyte resistance R_s for conduction through the suspending medium with two capacitive impedances (C_{eq}) in series, associated with the electrical double layers and photoresist at each of the two electrodes. The total impedance Z_T is defined[29,30] by:

$$Z_T = R_s[1 + \frac{2}{j\omega C_{eq} R_s}] \quad (8)$$

Here $C_{eq} = [C_d C_{PR}/(C_d + C_{PR})]$, where C_d and C_{PR} are the capacitance of the electrical double layer and photoresist layer over the electrode, respectively. For electrodes of surface area S, with photoresist thickness of t and κ^{-1} as a measure of double-layer thickness, $C_d = \varepsilon\kappa S$ and $C_{PR} = \varepsilon t^{-1} S$. R_s is calculated approximating the conduction path as having length equal to gap size ($2x$) and a cross-section defined by electrode width and a measure of the double-layer thickness, κ^{-1}.

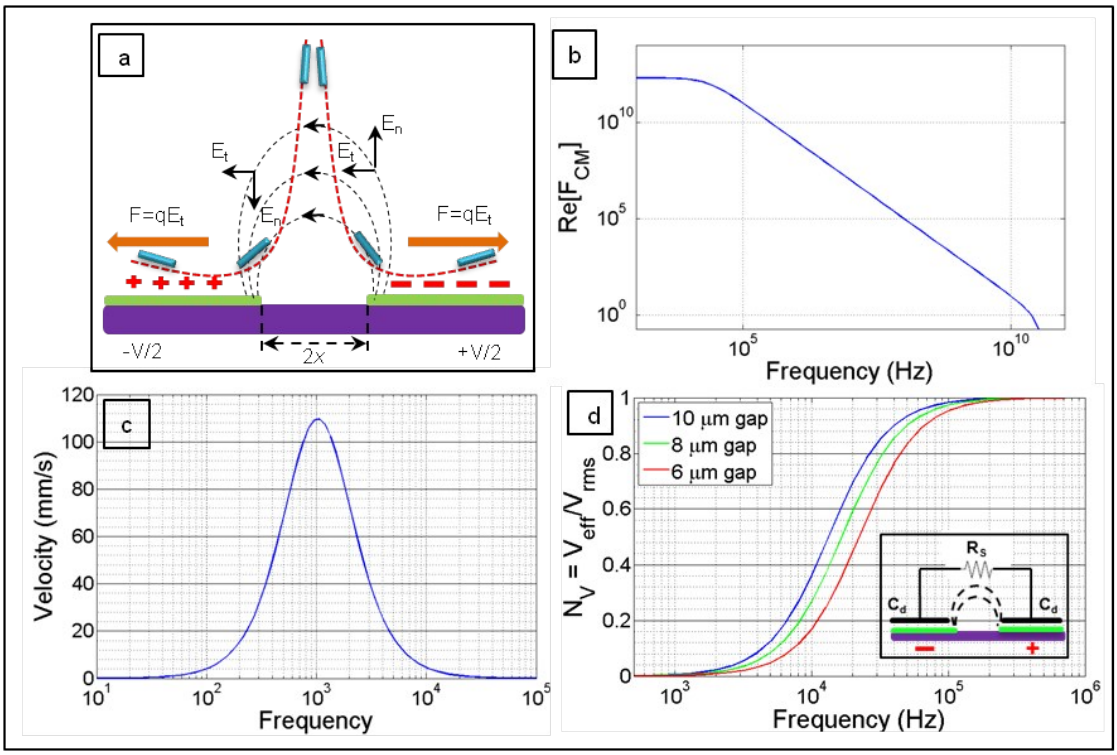

Fig. 3 Effect of frequency on director or disruptor forces: (a) Electroosmosis force (F) is a disruptor that drags NWs away from electrode gap. Frequency changes affect the competing director and disruptor forces by (b) altering the magnitude of DEP director force as a result of the change in the magnitude of $Re[F_{CM}]$ and (c) altering electroosmotic velocity of disruptor fluid vortices. (d) The ratio of the effective voltage to applied voltage for different gap sizes changes vs frequency due to electrode polarization (disruptor), modeled as an RC circuit (inset).

The ratio (V_{eff}/V_{rms}), the normalized effective voltage for DEP, may be defined, as seen in the inset of Fig. 3(d), by:

$$N_V = \frac{V_{eff}}{V_{rms}} = \left| \frac{1}{1+\frac{2}{j\omega R_s C_{eq}}} \right| = \frac{1}{\sqrt{1+(\frac{2}{\omega R_s C_{eq}})^2}} \quad (9)$$

The minimum normalized effective voltage for DEP ($N_V = 0$) occurs when the electrode polarization disruptor effect is maximum and vice versa. Therefore, normalized electrode polarization is defined as:

$$N_{EP} = 1 - N_V \quad (10)$$

Fig. 3(d) shows that at frequencies less than 10^5 Hz only a fraction of applied voltage is available for NW positioning and below 10^3 Hz, N_V goes to zero as the value of N_{EP} approaches 1. As seen from a curve for any single value of gap size in Fig. 3(d), we may maximize the fraction of applied voltage available for DEP to $N_V = 1$ by increasing the frequency. Our choice of electrode gap size is determined by NW length and the constraint to avoid disruptive torque. How does this choice affect the strength of electrode polarization as a disruptor?

The effect of varying electrode gap size is seen in the curves in Fig. 3(d), which shows that electrode polarization vanishes at higher frequencies for smaller electrode gap size ($2x$). This effect can be explained by the effect of relaxation times defined by Bazant *et al.*[31] as $\tau_c = 2x\kappa^{-1}/D$ where D is the ion diffusivity. Larger gap widths ($2x$) require longer charging time τ_c, and a lower frequency must be used to achieve the same double-layer thickness. As seen in Fig. 3(d), if the same frequency is used for larger gaps, the effective voltage available for the DEP field is increased, reflecting the reduced double-layer thickness.

2.3 Experimental observation: effect of strongly-coupled disruptors on assembly yield

In the last section, we have shown that frequencies higher than 10^5 Hz would be required to eliminate both electroosmotic flow and electrode polarization disruptors. To see the effect of these disruptors on yield, pre-clamped yield was measured at two frequencies: {1} 10^4 Hz, at which theoretical results in Fig. 3(d) show that only ~16, 28 and 38% of applied voltage is effective for NW assembly for gap sizes of 6, 8 and 10 μm respectively, and {2} 10^5 Hz, where V_{eff} is almost equal to V_{rms}. If the theoretical results in Fig 3 (c) and (d) are accurate, pre-clamped assembly yield should show a significant increase at 10^5 Hz, compared to 10^4 Hz. Experimental results are shown in Table 1 and Fig.4

{1} After eliminating weakly-coupled disruptors by following the guidelines provided in Section 2.1, NW assembly between electrodes with gap sizes, $2x$, equal to 6, 8 and 10 μm, was observed at 10^4 Hz. Almost no assembly occurred at voltages less than 7 V (rms) at this frequency. Increasing applied voltage to the maximum value available to us, 7 V (rms), 15 to 20% of wells filled with NWs. For each gap size, V_{eff}/V_{rms} at 10^4 Hz (based on Fig. 3(d)) and experimental yield of pre-clamped NWs are shown in Table 1.

{2} The yield was then studied for a range of voltages between

Table 1 Pre-clamped experimental yield (Exp. yield) at 10^4 Hz and 7 V (rms). Theoretical V_{eff}/V_{rms} was calculated using Fig. 3(d).

Gap size (μm)	V_{eff}/V_{rms}	Exp. yield (%)
10	0.38	20
8	0.24	18
6	0.18	15

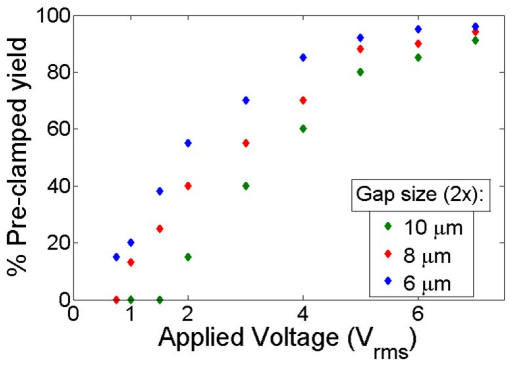

Fig. 4 Experimental results showing the effect of applied voltage on pre-clamped yield at 10^5 Hz for three different gap sizes ($2x$). Larger gap sizes have higher threshold voltage (2, 1 and less than 0.7 V (rms) respectively) for $2x$=10, 8 and 6 μm. Highest assembly yield occurs at 7 V (rms).

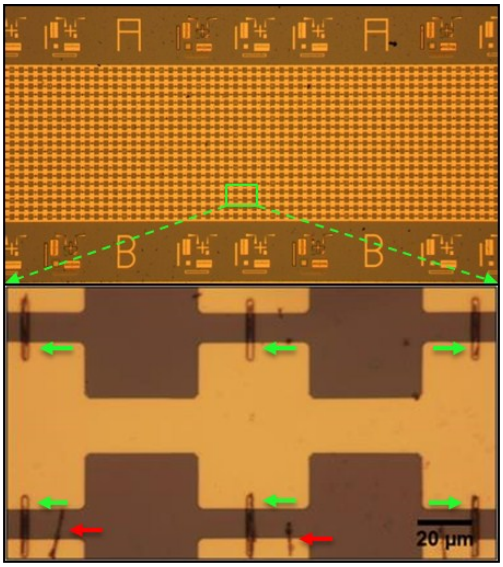

Fig. 5 Single NWs aligned in almost every well (green arrows) at 10^5 Hz and 7 V (rms). Red arrows show misaligned NWs.

0.7 to 7 V (rms) at 10^5 Hz as shown in Fig. 4. For each gap size, there is a threshold voltage below which NW assembly does not occur due to the small value of F_{DEP}. As seen in Fig. 4, NW assembly does not occur at voltages below 2, 1 and 0.7 V (rms) for 10, 8 and 6 μm gap sizes respectively. Increasing the applied voltage and resulting F_{DEP} increases the assembly yield. The maximum yield realizable, occurs at the highest available voltage of 7 V (rms) at 10^5 Hz. For this condition, we used two dies of 9500 sites, for each gap size. The measured pre-clamped yield varied with gap size. Several optical micrographs such as in Fig. 5, were used to determine the yield. The yields were 91% and 93 % for 6 μm gap, 94% and 95 % for 8 μm and 94% and 96 % for 10 μm gap size, resulting in an averaged pre-clamped yield of 94%.

2.4 Director-disruptor competition

To separate the director-dominant region from the region of competition, seen in Fig. 6(a) and (b), we introduce a cut-off frequency, at which the disruptive effects of normalized electroosmotic velocity and normalized effective voltage for DEP (N_V) are less than 5%. Normalized electroosmotic velocity N_{EO} is defined as:

$$N_{EO} = \frac{v}{v_{max}} = \frac{4\Omega^2}{(1+\Omega^2)^2} \tag{11}$$

where v_{max} defined in Sec 2.2.2, is the maximum electroosmotic velocity at EO-characteristic frequency. N_{EO} provides a non-dimensional measure of the strength of this disruptor.

Regions with frequencies greater than cut-off frequency are director-dominant regions. If the DEP force in this frequency range has magnitude sufficient to direct NWs, it will face negligible competition from disruptors in this region. Fig. 6(b) shows that when ethanol is used as the medium, a large disruptor-free frequency range is available, beginning at $\sim 10^5$ Hz and extending to $\sim 10^{10}$ Hz, the frequency for cross-over into the nDEP region.

The region with frequencies less than the EO-characteristic frequency (peak) is disruptor-dominant. Here high electrode polarization and electroosmotic fluid flow overcome the directive effect of DEP force and decrease the yield dramatically. At frequencies between cut-off and EO-characteristic frequencies, as seen in the central region of Fig. 6(a) and (b), directors and disruptors are competing. The cut-off and EO-characteristic frequencies vary as the medium changes, since both N_{EO} and N_V depend on the electrical properties of the medium. To investigate the effect of suspension medium properties, we chose water and ethanol and plotted N_{EO} and N_V vs frequency. Fig. 6(a) and (b) shows the three regions for water and ethanol respectively. The higher cut-off and EO-characteristic frequency for water compared with ethanol is due to the higher conductivity of water.

The competing region is an important region to study as the competition between forces can decrease or increase the device yield. How can the effect of competition between the director and the dominant remaining disruptors on device yield be approached quantitatively? As we have earlier (in Section 2.1) removed weakly-coupled disruptors, we now define a parameter, the yield index β, such that β=1 if there is no reduction of DEP by disruptors and β=0, if the disruptors are at their maximum value. β is defined as:

$$\beta = 1 - N_{EP} - N_{EO} \tag{12}$$

Using Eq. (10), this can be rewritten as:

$$\beta = N_V - N_{EO} \tag{13}$$

Fig. 6(c) and (d) shows how the region of competition and the

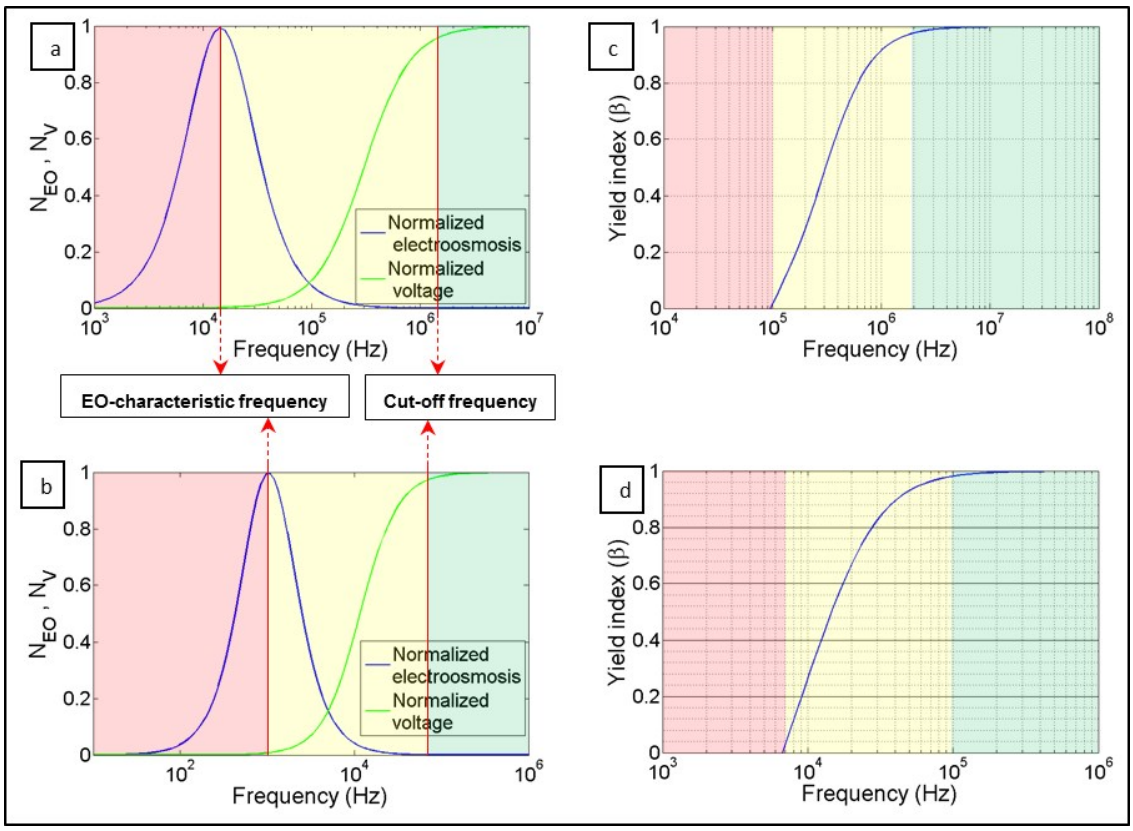

Fig. 6 Director-dominant (green), disruptor-dominant (pink) and competing region (yellow) for water (a) and ethanol (b) with electrical conductivity of 5×10^{-3} and 2.19×10^{-5} Sm^{-1} respectively. The yield index for water (c) and ethanol (d) indicates that a higher frequency is required for the effect of disruptors to be negligible in water, compared to ethanol. For this comparison, electrode gap size was 10 μm and 1μm photoresist layer was considered on the electrodes.

resulting yield index change with respect to frequency in water and ethanol respectively. For our selected parameter values, it shows that the yield index is maximum at frequencies higher than 2×10^6 Hz for water and 10^5 Hz for ethanol.

Fig. 6 enabled comparison of yield indices and operating parameters for suspension fluids -water and ethanol- with different properties. In this work, a layer of photoresist was coated on the electrodes (see Section 4.3). To calculate the yield index, the capacitance of the photoresist has to be included while calculating C_{eq} in Eq. (8). The resulting yield index with ethanol, plotted in Fig. 6(d), shows that the yield index increases slightly from 0.98 to 0.99, in moving from 10^5 to 2×10^5 Hz. However this frequency change would cause the term $\mathrm{Re}[F_{CM}]$ in the DEP force to decrease in value by nearly an order of magnitude from 6×10^{11} to 9×10^{10} (from the data used to create Fig 3(b)). In this case, to prevent large DEP force reduction, we select 10^5 Hz and forgo the small increase in yield index available at 2×10^5 Hz.

2.5 Clamping

Field-directed assembly typically requires clamping of the NWs, to secure them in place for a circuit or network (integration), or to build individually addressable NW devices. These may require, at one or both ends of a NW, electrical contact or a firm pedestal for nanomechanical applications of NWs. Here we briefly discuss clamping and post-clamped device yield. Methods such as electron beam induced deposition (EBID)[18] incur a cost proportional to the number of clamped devices; their cost becomes prohibitive for large arrays. Simultaneous electrodeposition of all required clamps on a chip, using the metal electrodes designed for DEP, circumvents this cost penalty. Electrodeposition of gold from cyanide-based solutions has been demonstrated in previous work with metal NWs[5] and with silicon NWs[15], to enable clamps of repeatable rigidity. Here, the use of silver (Ag) in place of gold enables a reduction in step cost (current cost ratio 1:65 for Ag:Au) and removes the dependence on toxic gold cyanide solutions. Fig. 7 shows a clamp fabricated to create a cantilevered NW with (inset showing) uniform interfacial contact of Ag.

Fig. 8 is selected to illustrate examples of defects -empty sites and NWs broken or misaligned during clamping in a high yield post-clamped array. More examples are provided in Fig. S4† and S5†. Other defects such as chained and multiple NWs are rarely seen, following our control of NW concentration. The inset shows a single clamped NW suspended about 500 nm above the electrode surface and free to serve as a mechanical resonator.

Since post-clamped yield can be lower than the yield from the assembly process alone, for a meaningful comparison of the results of different approaches, it is important to check which one is implied in published reports. For example, the 80% yield quoted in the work of Li *et al.*[15] refers to post-clamped yield and may be compared with the 88% yield in the current study. Freer *et*

Table 2 Table of comparison: identifying director and disruptor forces influencing the yield of single NW assembly in selected studies focused on increasing the yield of individually addressable single NWs. Effects marked by ‡ are classified as director or disruptor by us, based on qualitative information provided in the source. pDEP and nDEP refer to positive and negative dielectrophoresis.

Source	Director	Disruptor	Method
This work	• pDEP • Capillary inside wells	• nDEP • High NW concentration • Capillary at drying front • Electroosmosis • Electrode polarization • Low pDEP at very high frequency • Electrothermal fluid flow	Analytical & experimental
Collet *et al.* [19]	• pDEP • Capillary	• Very high pDEP • Electrode polarization ‡	Analytical & experimental
Palapati *et al.* [18]	• Low DEP force at pDEP to nDEP transition frequency	• Electrode polarization	Computational & experimental
Freer *et al.* [12]	• Hydrodynamic drag force in microfluidic channels • pDEP • Electrostatic repulsion between NW-NW and NW-electrode	• Very high pDEP • Hydrodynamic drag force in microfluidic channels	Analytical & experimental
Burg *et al.* [20]	• pDEP	• Electrothermal fluid flow • Electroosmosis	Computational & experimental
Raychaudhuri *et al.* [14]	• pDEP	• Electroosmosis • Electrode polarization • Low pDEP at very high frequency	Analytical & experimental
Li *et al.* [15] Smith *et al.* [13]	• pDEP • Capillary inside wells	•Electrode polarization‡ • Capillary in drying front‡	Analytical & experimental
Boote and Evans [9]	• pDEP	• Very high pDEP • Electrode polarization‡	Analytical & experimental

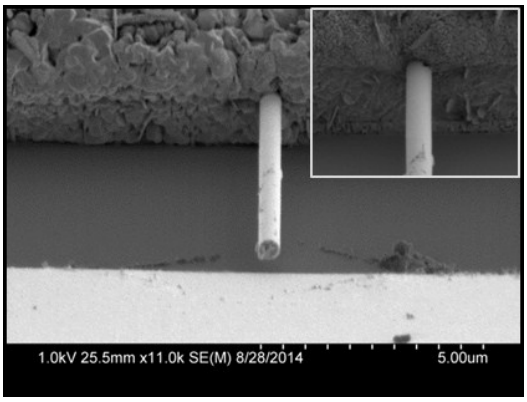

Fig. 7 Single-end-clamped nanoresonator using electrodeposited silver as clamp material, with inset showing the uniformity of the silver clamp around the NW.

al. [12] and Collet *et al.* [19] each introduce innovations, with new directors for yield enhancement. Using microfluidic channel flow [12] and capillary force [19], yields of 98.5% and 81% respectively, are reported by these groups. These studies do not attempt clamping, hence, the numbers from these studies should be compared with the pre-clamped yield of 94% in this work.

2.6 Towards a generalized director-disruptor framework

The entry to the literature on electrohydrodynamic (EHD) field-directed assembly of NWs to date may seem daunting to a new user. This comes from the fact that a number of effects such as DEP, electroosmosis, electrode polarization and electrothermal are involved, with varying roles reported in different studies. A few examples listed in Table 2, show that the same effect can serve either as a director or disruptor. For example, capillary force at moving front is a disruptor in this work and a director in [19]; positive DEP (pDEP), the main director for all studies, can be a disruptor at high magnitudes [9,12,19] as it can cause NW to attach on the electrodes instead of in the gap between them [19] or lead to positioning more than one NW between electrodes [9,12]; low pDEP is identified as a director in [18] and a disruptor in [14] and in our study. The intensity of each effect as well as its degree of coupling to others, varies in these studies. Further, each one of several physical parameters such as geometry, material properties and frequency and magnitude of applied voltage, can contribute to more than one effect.

The focus of this study is the introduction of a general framework for field-directed NW assembly processes, not limited to DEP, which will help to choose parameter values to maximize device yield. For any field-directed assembly process we propose a systematic procedure with the steps listed below. Sections of this paper where the work done serves as an example for each step, are noted in parenthesis below:

1. List the relevant effects and identify the physical parameters involved for each one. See Sections {2.1 and 2.2}.

2. Identify each effect as a possible director or disruptor. Sections {2.1 and 2.2}.

3. Where possible, estimate which disruptors are too weak to be significant; discard them. Sections {2.1.4 and 2.1.5}.

4. Identify disruptors that are not strongly coupled to any director -remove them, wherever possible, by experimental modification. Sections {2.1.1, 2.1.2 and 2.1.3 }.

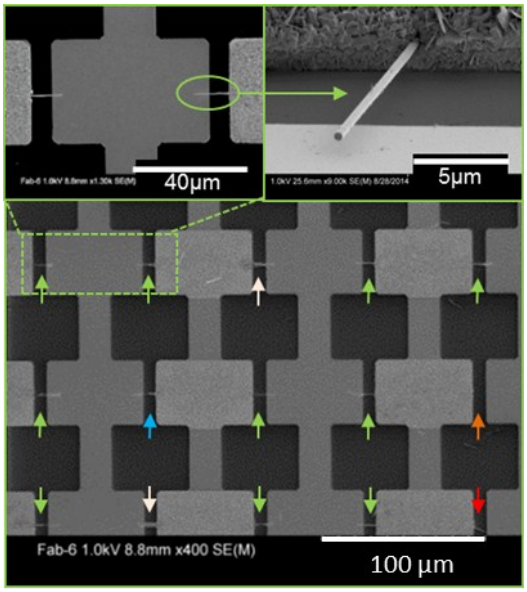

Fig. 8 High yield clamped single NW and defects. Green arrows: perfectly positioned and clamped NWs; blue arrow: a broken NW after clamping and removing photoresist; white arrow: NW bundle instead of single NW; orange arrow: no NW; red arrow: misaligned NW.

5. Examine remaining effects for which director-disruptor coupling could be strong -typically where both are either increased or decreased by the same change in any single physical parameter. Section {2.2}.

6. Use physical intuition, experiments, analysis or computation, to seek a minimal set of the simplest non-dimensional parameters that represent the competition between the remaining directors and disruptors well enough to be indicators of yield. Section {2.4}.

For the example protocol of DEP discussed in this work, using steps 1 to 6, we found that a single non-dimensional parameter, the yield index, can be used to represent the competition between the director (pDEP) and the strongly-coupled disruptors (electroosmosis and electrode polarization).

The number for the yield index should *not* be interpreted as the expected value of pre-clamped NW yield -*e.g.* a yield index of 0.94 is not the same as an expectation of 94% pre-clamped yield. The yield index β we have defined has value 1 if the disruptors are negligible and value 0 if the disruptors dominate and prevent DEP from functioning. The value of β is a guide which tells us how to move in the direction of disruptor reduction. We first determined frequency (here, 10^5 Hz) to make β close to 1. Further increase in the frequency would yield small disruptor reduction, but it would significantly reduce the DEP force due to reduction of $Re[F_{CM}]$ as discussed in Section 2.4. Therefore, we fixed the frequency. In order to increase the DEP force to try and achieve the best yield possible, the applied voltage was increased, as shown in Fig 4.

Aside from the primary use of the yield index discussed above, we note that the framework with resulting equations, can be useful even after a good working set of parameters for high yield index is finalized, and a high yield experimentally confirmed. Experimental considerations other than those related to the DEP assembly, may impose a new constraint on one of the parameters such as electrode gap size, property of the medium, or the frequency of the field. Considerable effort would be required to arrive at a new set of parameter values by experimental trial-and-error alone. Following the steps of the framework and equations given in Sections 2.1, 2.2 and 2.4, one can quickly obtain working estimates for remaining parameters, and use them to guide experiments confirming the best values.

This approach enabled a selection of physical parameters to significantly improve the post-clamped yield with respect to the earlier study of Li *et al.*[15] and obtain pre-clamped yield value close to the maximum yield reported to date by Freer *et al.*[12], but without the additional experimental cost and complexity of implementing microfluidic channels.

3 Conclusions and outlook

Field-directed assembly enables large-area coverage with individually addressable NW devices. The assembly cost is independent of area, with potential to aid nanoscale research and to open a path for nanomanufacturing. This study introduces a general director-disruptor framework of steps for any field-directed NW assembly process.

One of several directed assembly methods from the literature with positive dielectrophoresis as the main director was selected to serve as an example, to test the utility of the framework. We identified potential disruptors and estimated those that were weak, or weakly-coupled to the director. With guidance from analysis, computation, or experiment in this and earlier published work, we eliminated weak disruptors and defined constraints between variables for the weakly coupled disruptors. We then proposed a definition for a non-dimensional yield index, to capture the competition between the remaining disruptors and directors. The identification of constraints, as well as the definition of appropriate dimensionless parameters, improves intuition about the assembly process, reduces the dimension of parameter space and enables the determination of parameter values with far less trial-and-error. The values of several experimental parameters, such as electrode area and gap size, properties of the suspension medium and frequency of the applied field, were reflected in the yield index. Guided by the variation of the yield index, we obtained the maximum yield (88%) of functional (post-clamped) devices among published reports we have found in the literature to date.

The constraints and dimensionless parameters (such as the yield index here) should be determined afresh for any new field-directed assembly method. Once determined, they provide a rational path for selecting new parameter values, with greatly reduced trial-and-error, if any experimental parameter needs to be changed for reasons other than assembly process. In doing so, the director-disruptor framework has potential to serve as a vehicle for better understanding of the process, and for providing a rational, economical path towards design of a nanomanufacturing process for commercial and scientific use of large arrays of NW devices.

4 Experimental methods

4.1 Nanowire synthesis

Rh NWs were synthesized in porous membranes from an aqueous rhodium sulfate solution (RH221D from Technic). NWs with length up to 12 μm were synthesized by electrodeposition at -400 mV with respect to a Ag/AgCl reference electrode in 60 minutes[32]. Nanoporous AAO membranes with 200 nm nominal pore size and thickness of 60 μm (Whatman) and polycarbonate membranes with 400 nm nominal pore size and thickness of 20 μm (Sterlitech) were used for NW synthesis. NWs extracted from polycarbonate template are closer to a perfect cylinder than NWs synthesized in AAO templates. If this is important, the use of a polycarbonate templates is recommended. After dissolving the template (AAO by 3M NaOH and polycarbonate by dichloromethane), the NWs were suspended in ethanol. Electrodeposition experiments were controlled using a Princeton Applied Research VersaStat3 potentiostat/galvanostat. A detailed discussion of the NW synthesis is available in earlier work[32].

4.2 Nanowire concentration measurement

A known volume of NW suspension was dried on a silicon substrate. Fifty non-overlapping optical micrographs, including center and edge regions of the dried-out drop were analyzed using ImageJ software and the average was used to compute the total number of NWs in the sample. We found that concentrations above 3.3×10^8 NW/mL result in multiple layers or clumps of NWs on the substrate which does not allow for a credible count for NWs with this method. For assembly, we found that a concentration two orders of magnitude below this value was required to prevent chaining and multiple NWs per die. Hence, measurements of concentration made for the assembly are far below this limit.

4.3 Nanowire assembly

Six separate dies, each with 9500 NW assembly sites defined by electrode pairs with different gap sizes, were patterned using photolithography and metal lift-off on a silicon substrate with 300 nm of wet thermal oxide. Fig. 1 illustrates the patterning steps to which the following details apply: (a) patterning a $\sim$1 μm thick layer of deep ultraviolet (DUV) PMGI SF-11 photoresist (MicroChem) hard-baked (at 200°C for 5 min) to create wells for trapping NWs between each electrode pair. The wells are $\sim$500 nm deep with lengths of 12, 14 and 16 μm for electrode gap sizes of 6, 8 and 10 μm respectively (b) micro-pipetting 10 μL of suspension over each die, with AC voltage (frequency and voltage value determination discussed later) applied across all chosen electrode pairs to trap NWs within wells. A layer of Shipley 1811 photoresist (MicroChem), $\sim$1 μm thick was then spun and patterned to create a photoresist mask for exposing the PMGI layer over one electrode of each pair, to enable clamping of the NW end (c) electrodeposition of Ag, from Silver Cyless (succinimide) solution (Technic), to clamp one end of the NWs followed by removal of all photoresist and critical point drying.

PMGI photoresist was chosen in this process for several reasons. Ethanol dissolves Novolac-based photoresists such as Shipley 1811, but it does not dissolve the hard-baked PMGI photoresist. Therefore, the electric-field assisted NW assembly, using NW suspended in ethanol, was conducted on hard-baked PMGI as an insulating layer to prevent short circuit occurrence for the large-scale NW assembly. Finally, Shipley 1811 and hard-baked PMGI can be exposed at different wavelengths, enabling patterning of PMGI using DUV flood exposure through the Shipley mask.

The chief advantages of this fabrication sequence are: {a} capture of NWs at predetermined well locations {b} retention of NWs by capillary force at the surface of the evaporating medium inside the wells {c} removal of randomly scattered NWs with the photoresist in the last step. This fabrication method eliminates the disruptive effect of a high value of the dielectrophoretic (DEP) force, reported by Collet *et al.*[19], which causes undesirable NW attachment at several points on the electrodes.

The dielectrophoretic assembly process was performed using a Signatone 1160 probe station. A function generator (Tektronix CFG253) was used to apply frequencies up to 100 kHz and voltages up to 7 V (rms). A Canon 60D digital camera was used to observe the assembly of NWs. Post-clamped NWs were studied using Field Emission Scanning Electron Microscopy (FESEM, Hitachi S-4800).

4.4 Nanowire yield measurement

The percentage yield was computed from 500 out of 9500 randomly selected wells per die (3000 of 57000 wells per wafer). Optical micrographs provided in supplementary online documentation (Fig. S2† to S5†) show blank sites and other defects observed in the counting process. For measuring pre- and post-clamped yield, if multiple NWs were positioned between electrodes, only one NW per electrode pair was counted. Also, if a positioned NW bridged less than half the gap-width as shown in Fig. S4† , it was not counted.

Appendix

Scaling analysis -Brownian and dielectrophoretic displacement: Under the action of viscous drag force (F_d), given in Eq. (A-1), terminal velocity u is achieved when viscous drag force F_d opposing the motion becomes equal to applied DEP force F_{DEP}.

$$F_d = 4u\pi\eta L/[ln(2L/d)+0.5] \quad \text{(A-1)}$$

For a NW of mass m, the acceleration changes from $a = F_{DEP}/m = F_d/m$ to zero, as the velocity increases from zero to u. For a rough estimate of time scale,

$$\tau \cong \frac{u}{a} = \frac{\rho_p d^2}{16\eta}[ln(2L/d)+0.5] \quad \text{(A-2)}$$

For a rhodium NW with density ρ_p=12,410 Kg/m^3, L=10 μm, d=0.25 μm and ethanol dynamic viscosity $\eta=1.2\times10^{-3}$ kg/m.s, we calculate τ to be 1.2×10^{-7} s. Comparing this time to observation time $t\sim$1 s, the moving NW is almost always at terminal velocity. Using the relation for Brownian displacement with the Stokes-Einstein relation for particle diffusivity yields[22] $\Delta X_{Br} = (2k_BTt/\gamma)^{1/2}$. The displacement due to DEP force is

$\Delta X_{DEP} = ut = (F/\gamma)t$. The ratio of displacements, used in the order of magnitude analysis in Section 2.1.4, is then given by:

$$\Delta X_{Br}/\Delta X_{DEP} = \sqrt{(2K_BT)/(u^2\gamma t)} = \sqrt{(2K_BT\gamma)/(F^2 t)} \qquad \text{(A-3)}$$

5 Acknowledgments

This work was supported by grants from the Natural Sciences and Engineering Research Council of Canada (NSERC) Discovery and RTI programs, as well as from the Canada Foundation for Innovation (CFI)and British Columbia Knowledge Development Fund (BCKDF). It made use of the 4D LABS shared facilities supported by CFI, BCKDF, as well as Western Economic Diversification Canada (WD), and Simon Fraser University (SFU).

References

1 J. Chaste, A. Eichler, J. Moser, G. Ceballos, R. Rurali and A. Bachtold, *Nature Nanotechnology*, 2012, **7**, 301–304.
2 E. Sage, A. Brenac, T. Alava, R. Morel, C. Dupré, M. S. Hanay, M. L. Roukes, L. Duraffourg, C. Masselon and S. Hentz, *Nature Communications*, 2015, **6**, 6482–6487.
3 B. Ilic, Y. Yang, K. Aubin, R. Reichenbach, S. Krylov and H. Craighead, *Nano Letters*, 2005, **5**, 925–929.
4 A. Heidelberg, L. T. Ngo, B. Wu, M. A. Phillips, S. Sharma, T. I. Kamins, J. E. Sader and J. J. Boland, *Nano Letters*, 2006, **6**, 1101–1106.
5 M. Li, T. S. Mayer, J. A. Sioss, C. D. Keating and R. B. Bhiladvala, *Nano Letters*, 2007, **7**, 3281–3284.
6 X. Wu, J. S. Kulkarni, G. Collins, N. Petkov, D. Almécija, J. J. Boland, D. Erts and J. D. Holmes, *Chemistry of Materials*, 2008, **20**, 5954–5967.
7 R. B. Bhiladvala and Z. J. Wang, *Physical Review E*, 2004, **69**, 036307–5.
8 W. Lu and C. M. Lieber, *Journal of Physics D: Applied Physics*, 2006, **39**, R387–R406.
9 J. Boote and S. Evans, *Nanotechnology*, 2005, **16**, 1500–1505.
10 J. A. Sioss, R. B. Bhiladvala, W. Pan, M. Li, S. Patrick, P. Xin, S. L. Dean, C. D. Keating, T. S. Mayer and G. A. Clawson, *Nanomedicine: Nanotechnology, Biology and Medicine*, 2012, **8**, 1017–1025.
11 N. P. Dasgupta, J. Sun, C. Liu, S. Brittman, S. C. Andrews, J. Lim, H. Gao, R. Yan and P. Yang, *Advanced Materials*, 2014, **26**, 2137–2184.
12 E. M. Freer, O. Grachev, X. Duan, S. Martin and D. P. Stumbo, *Nature Nanotechnology*, 2010, **5**, 525–530.
13 B. D. Smith, T. S. Mayer and C. D. Keating, *Annual Review of Physical Chemistry*, 2012, **63**, 241–263.
14 S. Raychaudhuri, S. A. Dayeh, D. Wang and E. T. Yu, *Nano Letters*, 2009, **9**, 2260–2266.
15 M. Li, R. B. Bhiladvala, T. J. Morrow, J. A. Sioss, K.-K. Lew, J. M. Redwing, C. D. Keating and T. S. Mayer, *Nature Nanotechnology*, 2008, **3**, 88–92.
16 M. C. Wang and B. D. Gates, *Materials Today*, 2009, **12**, 34–43.
17 D. Whang, S. Jin, Y. Wu and C. M. Lieber, *Nano Letters*, 2003, **3**, 1255–1259.
18 N. K. Palapati, E. Pomerantseva and A. Subramanian, *Nanoscale*, 2015, **7**, 3109–3116.
19 M. Collet, S. Salomon, N. Y. Klein, F. Seichepine, C. Vieu, L. Nicu and G. Larrieu, *Advanced Materials*, 2014, **27**, 1268–1273.
20 B. R. Burg, V. Bianco, J. Schneider and D. Poulikakos, *Journal of Applied Physics*, 2010, **107**, 124308–11.
21 A. Maijenburg, M. Maas, E. Rodijk, W. Ahmed, E. Kooij, E. Carlen, D. Blank and J. Ten Elshof, *Journal of Colloid and Interface Science*, 2011, **355**, 486–493.
22 Y. Liu, J.-H. Chung, W. K. Liu and R. S. Ruoff, *The Journal of Physical Chemistry B*, 2006, **110**, 14098–14106.
23 A. Castellanos, A. Ramos, A. Gonzalez, N. G. Green and H. Morgan, *Journal of Physics D: Applied Physics*, 2003, **36**, 2584–2597.
24 J. Happel and H. Brenner, *Low Reynolds number hydrodynamics: with special applications to particulate media*, Noordhoff International, 1973, vol. 1.
25 J. Luecke and R. L. McCormick, *Energy & Fuels*, 2014, **28**, 5222–5228.
26 T. B. Jones, *Electromechanics of particles*, Cambridge University Press, New York, 1995.
27 N. G. Green, A. Ramos, A. Gonzalez, H. Morgan and A. Castellanos, *Physical Review E*, 2000, **61**, 4011.
28 M. Z. Bazant, *Electrokinetics and electrohydrodynamics in microsystems*, Springer Science, 2011, vol. 530.
29 B. C. Gierhart, D. G. Howitt, S. J. Chen, R. L. Smith and S. D. Collins, *Langmuir*, 2007, **23**, 12450–12456.
30 P. Mirtaheri, S. Grimnes and O. G. Martinsen, *Biomedical Engineering, IEEE Transactions on*, 2005, **52**, 2093–2099.
31 M. Z. Bazant, K. Thornton and A. Ajdari, *Physical Review E*, 2004, **70**, 021506–24.
32 N. Moghimian, M. Sam and R. B. Bhiladvala, *Materials Letters*, 2013, **113**, 152–155.